



Article

Construction and Method Study of the State of Charge Model for Lithium-Ion Packs in Electric Vehicles Using Ternary Lithium Packs as an Example

Yinquan Hu ^{1,*}, Heping Liu ² and Hu Huang ³

¹ School of Intelligent Manufacturing & Transportation, Chongqing Vocational Institute of Engineering, Chongqing 402260, China

² School of Electrical Engineering, Chongqing University, Chongqing 400044, China; engineer@cqu.edu.cn

³ Seres Group Co., Ltd., Chongqing 400000, China; huanghu@mjc-edu.cn

* Correspondence: hyq9812@cqvie.edu.cn

Abstract: Accurate and real-time estimation of pack system-level chips is essential for the performance and reliability of future electric vehicles. Firstly, this study constructed a model of a nickel manganese cobalt cell on the ground of the electrochemical process of the packs. Then, it used methods on the grounds of the unscented Kalman filter and unscented Kalman particle filter for system-level chip estimation and algorithm construction. Both algorithms are on the ground of Kalman filters and can handle nonlinear and uncertain system states. In comparative testing, it can be seen that the unscented Kalman filter algorithm can accurately evaluate the system-level chip of the nickel manganese cobalt cell under intermittent discharge conditions. The system-level chip was 0.53 at 1000 s and was reduced to 0.45 at 1500 s. These results demonstrate that the evaluation of the ternary lithium battery pack's performance is time-dependent and indicate the accuracy of the algorithm used during this time period. These data should be considered in the broader context of the study for a comprehensive understanding of their meaning. In the later stage, the estimation error of the recursive least-squares unscented Kalman particle filter method for system-level chips began to significantly increase, gradually exceeding 1%, with a corresponding root-mean-square error of 0.002171. This indicates that the recursive least-squares optimization algorithm, the unscented Kalman particle filter algorithm, diminished its root mean square error by 27.59%. The unscented Kalman filter and unscented Kalman particle filter are effective in estimating the system-level chip of nickel manganese cobalt cells. However, UPF performs more robustly in handling complex situations, such as pack aging and temperature changes. This study provides a new perspective and method that has a high reference value for pack management systems. This helps to achieve more effective energy management and improve pack life, thereby enhancing the reliability and practicality of electric vehicles.

Keywords: nickel manganese cobalt (NMC) cell; unscented kalman filter (UKF); unscented particle filter (UPF); state of charge (SOC); unscented particle (UP)



Citation: Hu, Y.; Liu, H.; Huang, H. Construction and Method Study of the State of Charge Model for Lithium-Ion Packs in Electric Vehicles Using Ternary Lithium Packs as an Example. *World Electr. Veh. J.* **2024**, *15*, 43. <https://doi.org/10.3390/wevj15020043>

Academic Editors: Joeri Van Mierlo, Yonggang Liu, Xiaopeng Tang and Quanqing Yu

Received: 9 November 2023

Revised: 15 December 2023

Accepted: 22 January 2024

Published: 30 January 2024



Copyright: © 2024 by the authors. Licensee MDPI, Basel, Switzerland. This article is an open access article distributed under the terms and conditions of the Creative Commons Attribution (CC BY) license (<https://creativecommons.org/licenses/by/4.0/>).

1. Introduction

Under the increasing environmental awareness and energy crisis, the advancement of electric vehicles (EVs) is a global focus of attention [1,2]. However, despite the significant advantages of EVs in eliminating exhaust emissions, reducing carbon footprint, and improving energy efficiency, the challenges of their large-scale application remain numerous, including issues of power storage and EV travel restrictions [3,4]. Among all energy storage devices, lithium-ion packs (LIPs) are extensively utilized in EVs, due to their excellent performance, becoming an important bridge connecting the power grid and EVs [5,6]. Nickel manganese cobalt (NMC), in particular, is the most commonly used type, and their excellent capacity, energy density, and durability make them dominant in EVs.

On the basis of these, the use of the unscented Kalman filter (UKF) and the unscented particle filter (UPF) to evaluate and optimize the model is proposed for the first time. It is a brand-new perspective and method that helps measure and predict the state and performance of the battery more accurately. It is crucial to understand the state of charge (SOC) of the packs during the operation of EVs. The SOC is the most commonly used pack health indicator that can describe the ratio of the current pack's remaining capacity to total capacity. It belongs to the most important monitoring parameters in the battery management system (BMS). However, due to the complexity of internal chemical reactions in packs, the accuracy and real-time performance of the SOC, which is currently widely accepted and applied, cannot meet the pursuit of pack performance in existing EVs. In recent years, there has been rapid development in artificial intelligence, and the widespread application of machine learning algorithms in SOC estimation has led to greater development in data-driven methods. Xin et al. proposed using machine learning combined with multi-step prediction strategies to improve the accuracy of the multi-step prediction of the SOC. They also studied the effects of different multi-step prediction strategies using actual LPA data. The outcomes indicate that the actual SOC prediction of LPAs exhibits significant linear characteristics during the charging process, while the discharge process exhibits nonlinear characteristics [7]. Li et al. used the adaptive extended Kalman filtering algorithm (KFA) to correct the noise when estimating the SOC using the extended KFA. The relevant outcomes demonstrate that this method could markedly improve the accuracy of SOC estimation. Under dynamic stress testing conditions, the estimation accuracy was improved by 2%. Under the dynamic stress testing conditions of pure electric buses in Beijing, the estimation accuracy was improved by 0.39% [8]. In this study, the evaluation methods based on UKF and UPF were used to evaluate and optimize the model. Both the UKF and UPF algorithms are on the ground of Kalman filters and are suitable for handling nonlinear and uncertain system states. This new design method is not only used to estimate the effectiveness of SOC estimation for ternary LPA EVs, but, the research also found that this method is helpful for achieving more effective energy management, improving battery life, and enhancing the reliability and practicability of EVs, factors not involved in previous research. This can achieve more effective energy management, improve pack life, and enhance the reliability and practicality of EVs to a greater extent. It provides new ideas for the market-oriented and large-scale production and application of EVs. This study will be conducted in four parts. The first part is an overview of the construction of a SOC model and the research methods for LIPs in EVs. The second part is the model for constructing a SOC model and researching methods for LIPs in EVs. The third part is the experimental verification of the second part. The fourth part is a summary of the research content and points out the shortcomings.

2. Materials and Methods

The system-level chip can integrate various battery management functions, including battery charge and discharge control, battery SOC estimation, etc. This integrated design can enhance the stability and reliability of the BMS and improve the accuracy of SOC estimation through optimization algorithms. Building a ternary LPA SOC model is a core component of the pack management system. The primary task is to set the parameters of the model and adjust and optimize the model to be closer to reality. Next, two valuation methods are introduced: the UKF-based valuation and the UPF-based valuation. To accurately calculate the pack's SOC and dynamically adjust the state, the LPA SOC is accurately estimated by utilizing nonlinear uncertain system states. Then it comprehensively utilizes particle filters and Kalman filters to make the estimation more accurate and less risky.

2.1. Construction of a Ternary LPA Model

Due to the fact that the SOC of the power LPA cannot be directly measured by instruments and can only be indirectly estimated by measuring parameters, such as the voltage, current, and temperature, of the packs under certain experimental conditions,

it is particularly important to choose a suitable and effective pack model. This directly influences the accuracy of the estimated pack SOC [9,10]. To comprehensively reflect the impact of factors such as the charge–discharge rate, temperature, and capacity changes on accurately evaluating the SOC of the LPA, the SOC of the ternary LPA is defined, as shown in Equation (1).

$$\text{SOC}(t) = \text{SOC}_0 - \int_0^t \frac{\eta i(\tau)}{C(T, \kappa, t)} d\tau \quad (1)$$

In Equation (1), η is the charging and discharging rate. T serves as the pack temperature. $C(T, \kappa, t)$ is the available capacity of the ternary LPA at different temperatures and charge–discharge rates after discretization, as shown in Equation (2).

$$x_k = x_{k-1} - \left(\frac{\eta \Delta t}{C} \right) i_{k-1} \quad (2)$$

In Equation (2), x_k is the SOC of the ternary LPA at time k . i_{k-1} represents the operating current of the ternary LPA at time $k - 1$, and Δt represents the time interval [11,12]. Combining the dual polarization (DP) model, the state space model of the ternary packs is shown in Equation (3).

$$\begin{bmatrix} \dot{U}_m \\ \dot{U}_n \\ \text{SOC} \end{bmatrix} = \begin{bmatrix} -\frac{1}{R_m C_m} & 0 & 0 \\ 0 & -\frac{1}{R_n C_n} & 0 \\ 0 & 0 & 0 \end{bmatrix} \begin{bmatrix} U_m \\ U_n \\ \text{SOC} \end{bmatrix} + \begin{bmatrix} \frac{1}{C_m} \\ \frac{1}{C_n} \\ \frac{\eta}{C} \end{bmatrix} \quad (3)$$

In Equation (3), U_m and U_n are the voltages at both ends of the RC parallel branch. C serves as the maximum usable capability of a ternary LPA. The working voltage of the port is obtained by combining the composite model with the parallel voltage of two polarization effects in the DP model. Under normal circumstances, EVs are constantly providing new input and output data, and this constantly updated information should be utilized to improve the performance of vehicle mileage prediction. Online identification of model parameters is needed to optimize the estimation. One of the most widely used methods for identifying or estimating parameter values is the least-squares method, which can be used to fit and characterize the statistical characteristics of the estimated parameters for a set of data functions. There are important elements that affect the capacity of the LPA, such as the charge–discharge rate, temperature, etc. The DP model can quantitatively characterize the electrochemical polarization effect and the concentration polarization effect of the LPA simultaneously, achieving the basic requirements superior to the Thevenin model in terms of accuracy. In addition, combined with the composite model, the accuracy is greatly improved, compared to other pack models that consider a single factor. The DP composite model established in this article has the basic characteristics of being simple, convenient, and easy to operate, with little computational complexity. It is relatively easy to implement in engineering applications and can accurately identify model parameters. Large amounts of voltage, current, and SOC data can be obtained in the charging and discharging tests of the LPA. On the grounds of these data, the RLS method is utilized for identifying the model parameters [13,14]. The recursive formula using the least-squares method is showcased in Equation (4).

$$\left\{ \begin{array}{l} \hat{\theta}(k) = \hat{\theta}(k-1) + K(k)(e(k) - \zeta^T(k)\hat{\theta}(k-1)) \\ \hat{\theta} = (E_0, R_c, R_d, k_0, k_1, k_3)^T \\ K(k) = \frac{P(k-1)\zeta(k)}{1 + \zeta^T(k)P(k-1)\zeta(k)} \\ P(k) = (1 - K(k)\zeta^T(k))P(k-1) \end{array} \right. \quad (4)$$

In Equation (4), $\hat{\theta}$ serves as the parameter vector to be identified. $K(\cdot)$ serves as the gain. $\zeta(\cdot)$ serves as the experimental data matrix. $P(\cdot)$ serves as the covariance matrix. $e(k)$ serves as the terminal voltage error. I is the identity matrix. The structural diagram of a ternary LPA is showcased in Figure 1.

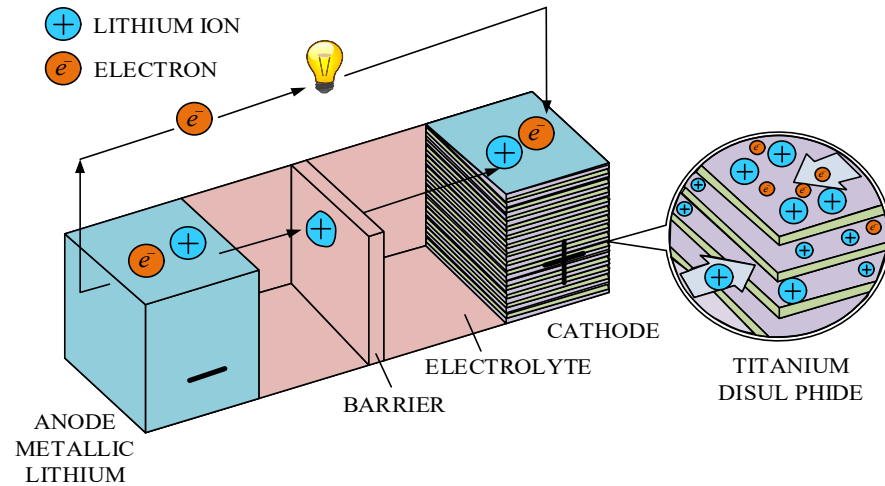


Figure 1. Structural diagram of a ternary LPA.

In Figure 1, a ternary LPA is a common type of LIP that consists of a positive electrode (PE), a negative electrode (NE), a separator, and electrolyte components. The PE is the PE plate in the ternary LPA, usually coated with active materials, such as lithium nickel manganese cobalt oxide (LiNiCoMnO_2), on the conductive collector. The main function of the PE is to receive and release lithium ions during the charging and discharging processes. The NE is the NE plate in a ternary LPA, usually coated with graphite material on a conductive collector. The function of the NE is to release and receive lithium ions in the charging and discharging processes. The diaphragm, made of polymer materials, acts as an isolation layer between the PE and NE plates. The diaphragm serves to isolate the PE and NE while allowing lithium ions to pass through in the charging and discharging processes. The electrolyte is a conductive medium in the ternary LPA, usually composed of lithium salts and organic solvents. The electrolyte contains lithium ions [15,16].

2.2. Estimation and Algorithm Construction of a Ternary LPA SOC on the Ground of UKF

Firstly, due to multiple factors, such as temperature and discharge current, the performance and lifespan of the ternary LPA will undergo significant changes during practical use. This study selected UKF as the SE algorithm. This algorithm is unique in handling the SOC estimation problem of multivariable nonlinear systems, such as the ternary LPA. It can effectively integrate various factors mentioned above and provide accurate estimates of the corresponding SOC [17,18]. The system state and measurement equation of the KFA are shown in Equation (5).

$$\begin{cases} x(k) = \phi_{k,k-1} \times x(k-1) + B_{k-1}u_{k-1} + \Gamma_{k-1}w(k-1) \\ y_k = C_k \times x(k) + D_k u_k + v(k) \end{cases} \quad (5)$$

In Equation (5), u_k is the input value at time k . y_k is the actual measured output value. Γ is a noise-driven array. $\phi_{k,k-1}$ serves as the transfer matrix. B_{k-1} serves as the input matrix

of the system. C_k serves as the output matrix. D_k serves as the feedforward matrix. v_k serves as the measurement matrix. The variance of process noise is shown in Equation (6).

$$\begin{cases} E[w_k w_k^T] = \begin{cases} Q_k & n = k \\ 0 & n \neq k \end{cases} \\ E[v_k v_k^T] = \begin{cases} R_k & n = k \\ 0 & n \neq k \end{cases} \end{cases} \quad (6)$$

In Equation (6), Q_k is the covariance of the process noise and serves as a non-negative definite matrix. R_k is the covariance of the measurement noise, which is a positive definite matrix. The difference between the UKF and extended Kalman filter method is that the UKF algorithm does not linearize the nonlinear equation but determines the sampling points near the estimated point by calculating the unscented transformation; it approximates the probability density function of the state variable with the Gaussian density corresponding to the sample points, achieving accurate estimation [19,20].

The unscented transform (UT) is a method for calculating the probability of nonlinearly transformed random vectors. It is incorporated into a deterministic sampling nonlinear algorithm on the ground of the Kalman linear filtering framework, known as the unscented KFA. The traceless transformation is the foundation and core content of the UKF algorithm, and the principle of UT transformation is shown in Figure 2.

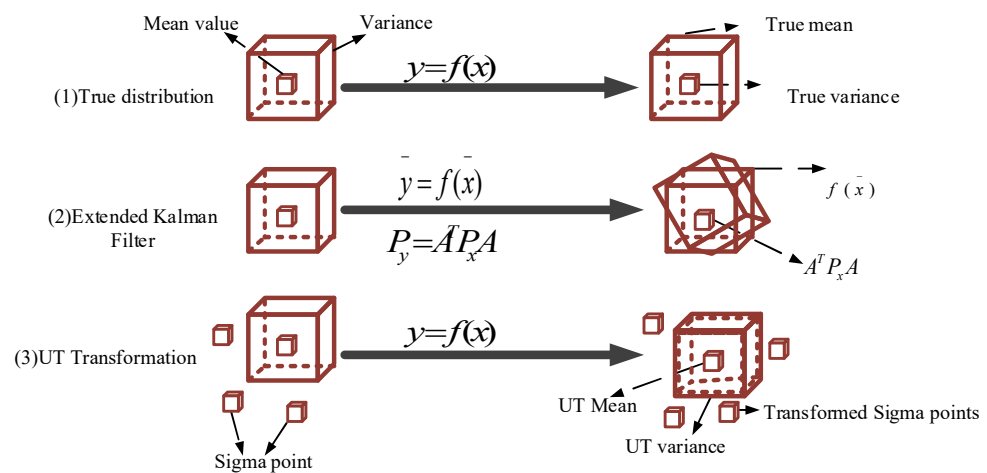


Figure 2. Schematic diagram of unscented transformation.

In Figure 2, the central idea of the traceless transformation is that the calculation process should prioritize ensuring that the sampling mean and covariance are \bar{x} and P_x , respectively. This set of sampling points is transformed nonlinearly for each sigma point to obtain the point sets \bar{y} and P_y , and the predetermined system is $y = f(x)$ [21,22]. The dimension of the state matrix is shown in Equation (7).

$$\begin{cases} x_i = \bar{x} \\ x_i = \bar{x} + \left(\sqrt{(n + \lambda)P_x}\right)_i \\ x_i = \bar{x} - \left(\sqrt{(n + \lambda)P_x}\right)_i \end{cases} \quad (7)$$

In Equation (7), \bar{x} and P_x are the mean and variance of the n -dimensional state variable x . X_i serves as the i th column of the variable matrix, and $\left(\sqrt{(n + \lambda)P_x}\right)_i$ serves as the i th column of the matrix $\sqrt{(n + \lambda)P_x}$. Generally speaking, when estimating the SOC of an LPA, the charging and discharging currents of the packs are used as the excitation input for the system to be tested, and the observed variable is the operating voltage of the system. After the system inputs excitation information, the observation will also track the estimated

state variables over time. Therefore, when utilizing the UKF algorithm to estimate the SOC of the NMC LPA, it is also necessary to first clarify the observed variables, state variables, and excitation inputs of the system. The initialization of state variables and covariance is shown in Equation (8).

$$\begin{cases} X_0 = E[x_0 \ w_0 \ v_0] = E[\text{SOC}_0 \ 0 \ 0]^T \\ P_0 = E[(x_0 - X_0)(x_0 - X_0)^T] \end{cases} \quad (8)$$

In Equation (8), x_k is the state variable. P_y is the covariance. Using the ampere hour integration method, the expression of the relationship between the SOC and the time can be obtained, as shown in Equation (9).

$$\text{SOC} = \text{SOC}(t_0) - \int_{t_0}^{t-t_0} \frac{I(t)}{C} dt \quad (9)$$

In Equation (9), the selection of initial values directly affects the overall filtering effect and has a decisive impact on the convergence speed (CSP) of Kalman filtering. On the grounds of the above derivation, a flowchart to evaluate the SOC of the LPA using the UKF algorithm is established, as showcased in Figure 3.

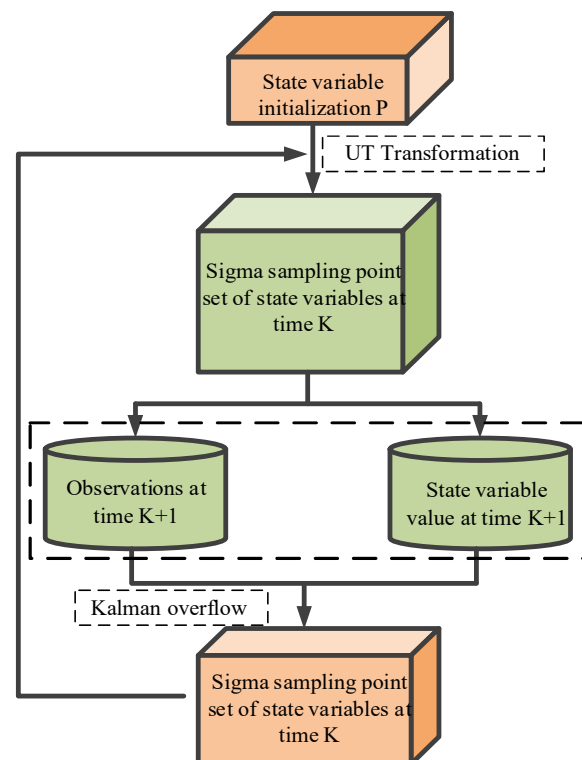


Figure 3. UKF algorithm estimation SOC flowchart.

In Figure 3, the DP model is selected as the pack model. The DP model has strong expressive power and can effectively simulate pack polarization phenomena and electrochemical processes. Once the model is established, the UKF can be used for estimating the SOC. The UKF is an efficient mechanism for handling nonlinear problems. Unlike direct linearization, the UT is used to approximate the effects of nonlinear functions at the mean and covariance, allowing the algorithm to have better performance when dealing with multivariate nonlinear systems. Finally, the constructed UKF-based SOC estimation algorithm is validated through a large amount of experimental data from the ternary LPA. The results met the expected accuracy requirements.

2.3. SOC Estimation and Algorithm Construction for the Ternary LPA on the Ground of UPF

The method of using the UKF for generating the importance distribution of PF is called UPF [23,24]. It establishes a mathematical model of the internal state of the packs, including the packs' voltage, temperature, charging current, etc. Then, experimental measurements are conducted to measure the discharge curve data of the packs under different states, which are input into the UPF filter for training and validation. The UPF combines the accuracy of the Kalman filter and the wide area of particle filter to optimize the handling of nonlinear and non-Gaussian problems. This is particularly applicable to the valuation of the ternary LPA SOC. The algorithm flowchart for estimating the SOC state of the ternary LPA using UPF is showcased in Figure 4.

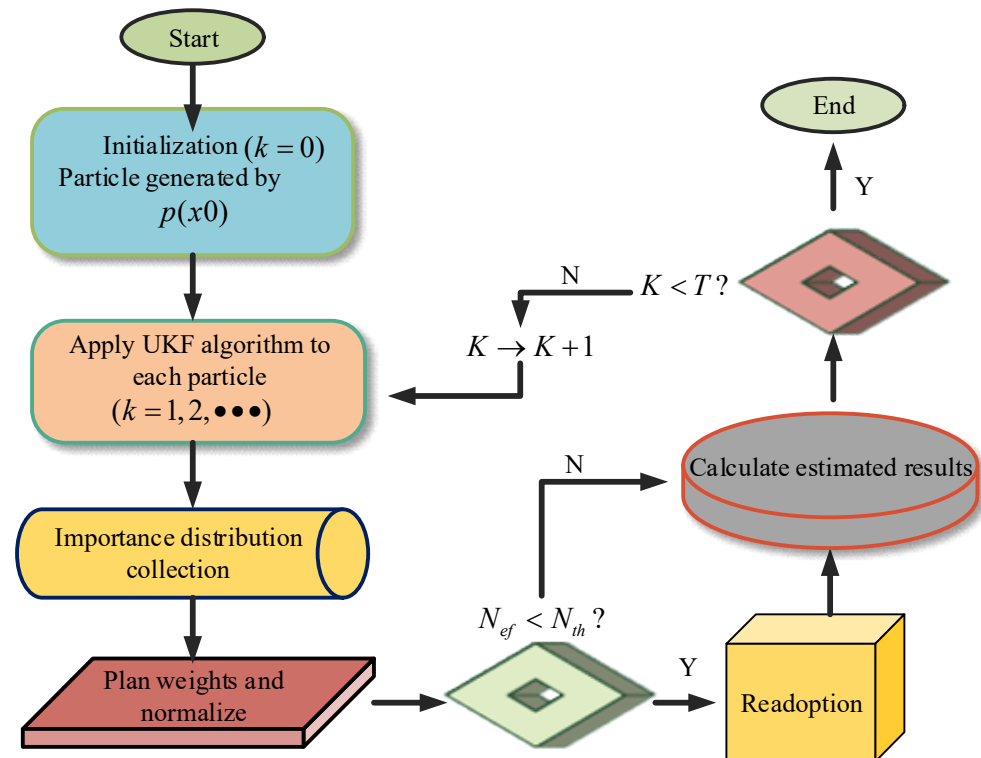


Figure 4. UPF algorithm estimation flowchart.

Firstly, the study initializes the number and weight of particles, using the set of these particles to approximate the posterior probability of nonlinear transformation. Then, by combining the characteristics of Kalman filtering, it predicts and updates the system as accurately as possible. The prediction stage relies on the distribution of particle weights and changes in the state equation to predict new particle states. Then, during the update phase, the particle weights are updated by measuring the difference between the predicted and actual outputs of the particles. To avoid particle degradation issues, resampling is conducted as the quantity of effective particles drops below a certain threshold. This helps to maintain the diversity of the particle set, thereby more accurately reflecting the system state. Finally, the estimation of the SOC is completed by combining the UPF and the ternary LPA models. The SOC value of the NMC packs is used as the state variable, and the open-circuit voltage OCV of the ternary LPA is used as the observation variable. It discretizes the state equation and observation equation of the ternary LPA model, as shown in Equation (10).

$$X_{k+1} = f(x_k, i_k, w_k) = H_k X_k + \psi_k i_k + w_k \quad (10)$$

In Equation (10), w_k serves as the system noise. ψ_k serves as the independent variable noise. It normalizes the voltage value of the pack's module, as shown in Equation (11).

$$\bar{q}_i = q_i / \sum_{j=1}^N q_j \quad (11)$$

In Equation (11), \bar{q}_i is the corresponding probability of the error covariance. It calculates the gain matrix of the filter, as shown in Equation (12).

$$K_k = P_{x_k, y_k} / P_{y, k}^{i-} \quad (12)$$

The root-mean-square error (RMSE) of SOC estimation is defined, as shown in Equation (13).

$$RMSE = \sqrt{\frac{\sum_{k=1}^N (\text{SOC}_k - \text{SOC}_{real, k})^2}{N}} \quad (13)$$

In Equation (13), N is the running time of one experiment. SOC_k is the estimated value of SOC in step k . $\text{SOC}_{real, k}$ is the true value in step k [18–20]. In response to the shortcomings of the EKF algorithm in generating recommendation distributions, this study uses the UKF algorithm to generate recommendation distributions for state variables. The algorithm is structurally on the ground of the UT transformation and uses Kalman linear filtering as the operational framework. The specific sampling form formed is deterministic sampling. It usually adopts symmetric sampling, with $2n+1$ sigma points. The UPF algorithm does not directly approximate nonlinear models but approximates the probability density function of state variables, avoiding the tedious calculation of Jacobi matrices while maintaining high estimation accuracy. Therefore, this article uses a UKF algorithm for generating an important density function and uses the unscented Kalman particle filter algorithm to estimate the SOC of the NMC LPA.

3. Results

It is inferred that the UKF and the UPF methods have greater potential in practical applications, but their relatively high computational complexities also need to be taken into account when conducting practical applications. It is necessary to further optimize and develop more feasible SOC valuation methods. Both algorithms could markedly evaluate the SOC of the ternary LPA, but there are significant differences in specific performance.

3.1. Analysis of SOC Estimation for the Ternary LPA on the Ground of UKF

At the beginning of the experiment, for the convenience of testing, the ternary LPA is discharged to a charge of 0.7 SOC in the pack testing equipment, and then the intermittent discharge condition is set. After the experiment begins, the experimental data is recorded in the software of the workstation. The initial state of the EKF algorithm is set to 75%, with initial state covariance, process noise Q_0 , measurement noise R , and a sampling time of 1 s. Then, it imports the test data into the program and estimates the SOC of the ternary LPA. It applies the UKF algorithm to estimate the SOC of the NMC ternary LPA, as shown in Figure 5.

Figure 5 showcases that the UKF algorithm could evaluate the SOC of the ternary LPA under intermittent discharge conditions. In addition, the SOC at 1000 s is 0.53, and at 1500 s, it is 0.45. This indicates that the estimation effect (EEF) is very good in the initial stage. The reaction speed is not particularly fast, verifying the general convergence characteristics of the UKF algorithm.

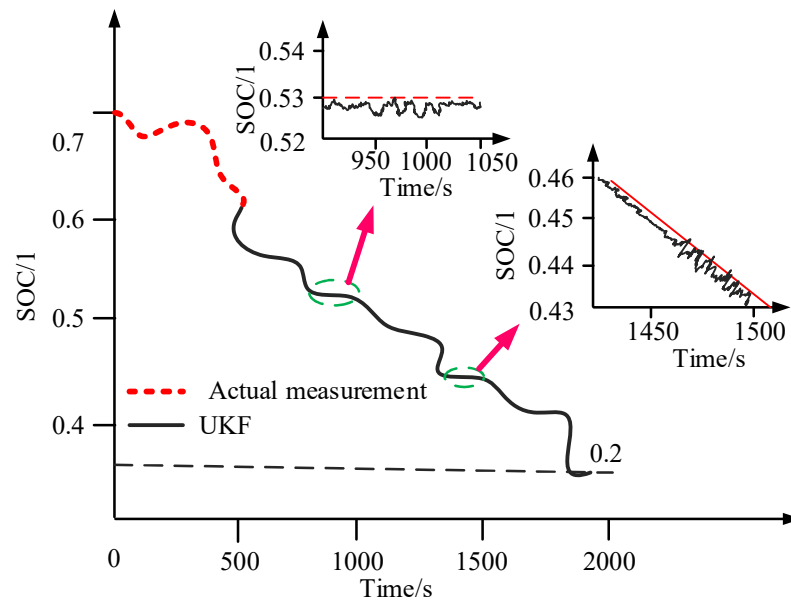


Figure 5. Estimation of the ternary LPA SOC on the ground of the UKF algorithm.

In practical applications, the convergence of the UKF algorithm is an important consideration. Although the UKF algorithm may require a longer convergence time, once converged, it can provide a relatively accurate SOC estimation. Therefore, the research results indicate that the UKF algorithm can serve as a reliable method for evaluating the SOC of the ternary LPA under intermittent discharge conditions. What needs further research is how to further improve the reaction speed of the UKF algorithm to adapt more quickly to changes in different working conditions. This is crucial for real-time monitoring and control in practical applications. By optimizing algorithm parameters and improving filter design, the performance, applicability, and accuracy of the UKF algorithm can be further improved. Overall, these results are meaningful for understanding and improving the application of the UKF algorithm in the estimation of the ternary LPA SOC and provide valuable clues for future research.

3.2. Analysis of SOC Estimation for the Ternary LPA on the Ground of UPF

To verify the superiority of the UPF algorithm in estimating the SOC performance of the LPA, intermittent discharge tests were conducted on a 3.7 V/3.2 Ah LPA produced by Panasonic. It recorded real-time data, such as the voltage and current of the ternary LPA at room temperature (25 °C), and the relevant data were utilized as the simulation input. The simulation design set the initial SOC value of the ternary LPA to 0.7 and the particle number to 200, and the test condition was the intermittent discharge test. The simulation time was set to 2000 s, and the sampling frequency was set to 2 Hz. This UPF algorithm is shown in Figure 6 under different parameter identification errors.

In Figure 6, in the same situation, the estimating outcomes of the two scenarios are basically the same at the beginning of a period of time. Nevertheless, in the later stage, the estimation error of the RLS-UPF method for the SOC began to significantly increase, gradually exceeding 1%, with a corresponding RMSE of 0.002171. This indicates that the ORLS-UPF algorithm decreased by 27.59%, compared to RMSE, indicating that the gap between the two will continue to widen over time. In short, the UPF algorithm on the ground of ORLS has the better SOC estimation performance. The comparison chart of SOC effects estimated by various algorithms is shown in Figure 7.

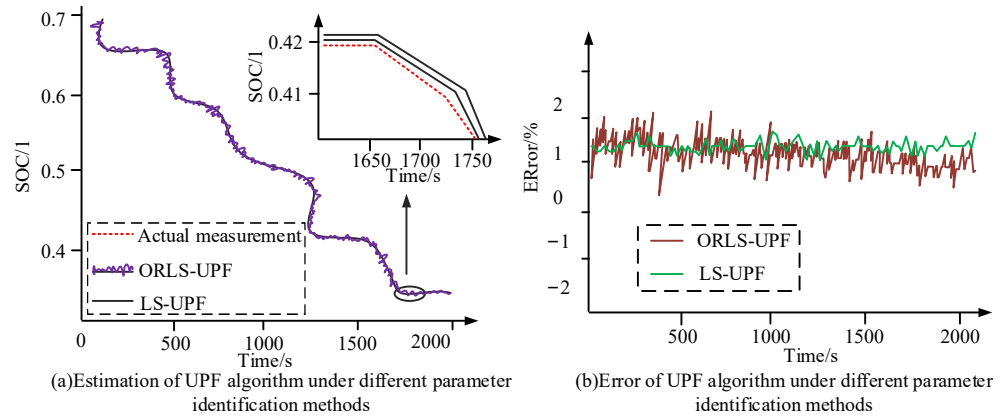


Figure 6. The SOC estimation error of the UKF algorithm under different identification errors of the parameters.

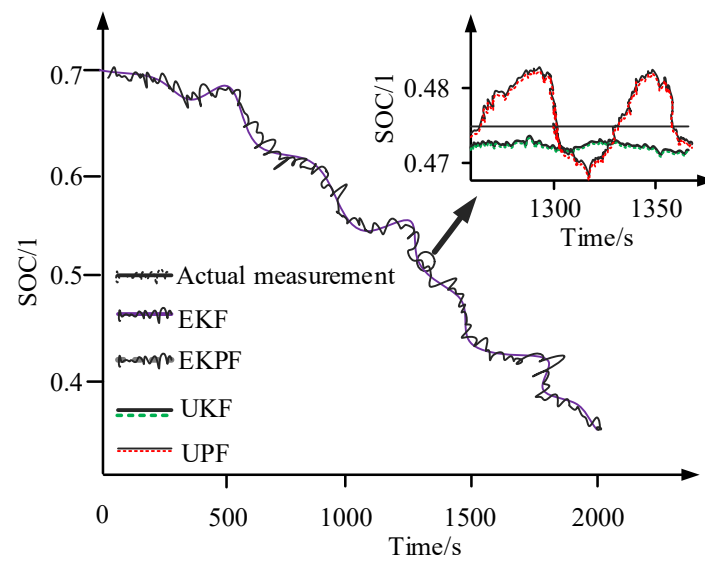


Figure 7. Comparison of the SOC effects of various algorithms for estimation.

In Figure 7, all four algorithms can better estimate the trend of SOC changes. However, it is evident that the SOC estimation method on the ground of the UPF algorithm possessed a significant improvement in the maximum absolute value of estimation error relative to the other three methods. The EKF was more excellent. Various algorithms estimated SOC errors, as shown in Figure 8.

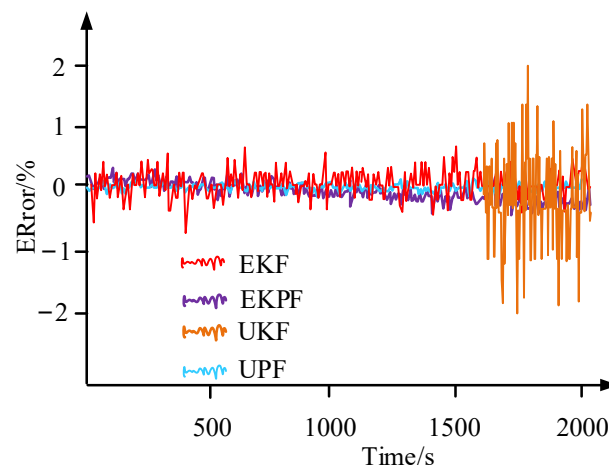


Figure 8. SOC error estimated by various algorithms when the initial value of SOC is 0.7.

In Figure 8, the overall analysis of RMSE performance comparison results shows that UPF increased by 50.9% compared to EKF, 33.4% compared to EKPF, and 19.6% compared to the UKF. The maximum absolute error was also controlled from around 3% of the EKF to within 1%, but it was relatively slow in running time. However, due to the continuous operation time of the system, it will not possess an essential influence on the actual SOC EEF. The robustness verification of the UPF algorithm is shown in Figure 9.

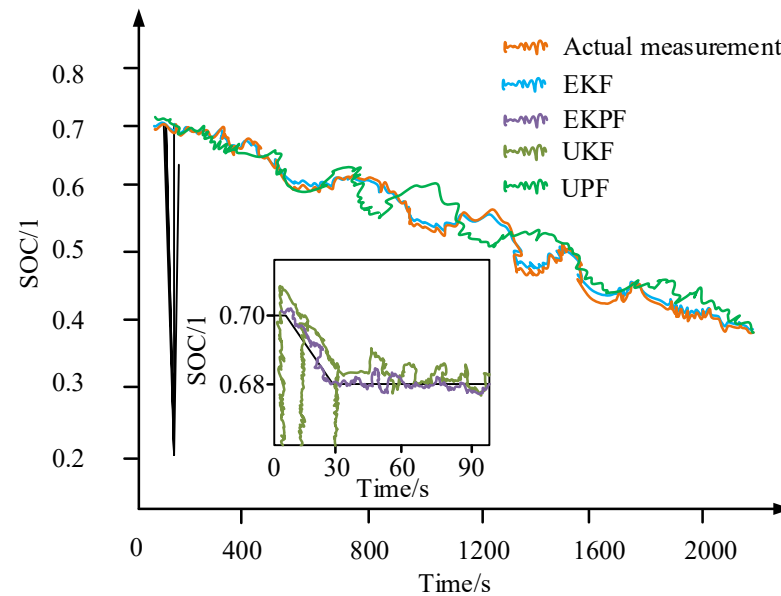


Figure 9. Robustness verification of the UPF algorithm.

In Figure 9, the CSPs of UPF and EKPF were the fastest; however, the error of UPF was below that of EKPF, and the convergence effect (CEF) was more stable. Moreover, the RMSE of UPF was the smallest, and it demonstrates that the CSP of UKF was slower. Therefore, relative to the other three algorithms, UPF possesses stronger robustness and interference suppression capability. The initial SOC value was 0.2, and the algorithm estimation error is shown in Figure 10.

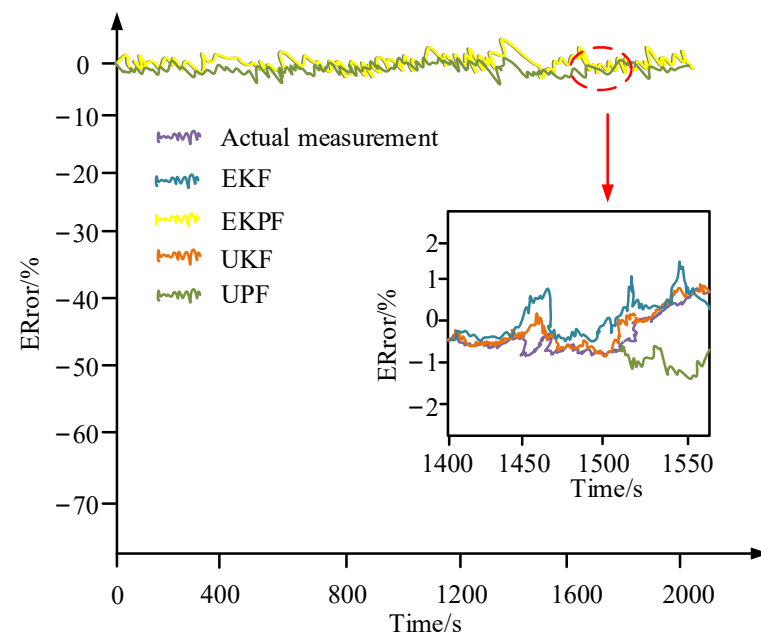


Figure 10. SOC error estimated by various algorithms when the initial value of SOC is 0.2.

In Figure 10, the CSPs of UPF and EKPF were the most rapid; however, the error of the UPF was below that of EKPF, and the CEF was more stable. Moreover, the RMSE of the UPF was the smallest, and it demonstrates that the CSP of the UKF was slower. Therefore, relative to the others, the UPF possesses a stronger robustness and interference suppression capability. The algorithm estimation robustness at an initial SOC value of 0.2 is shown in Figure 11.

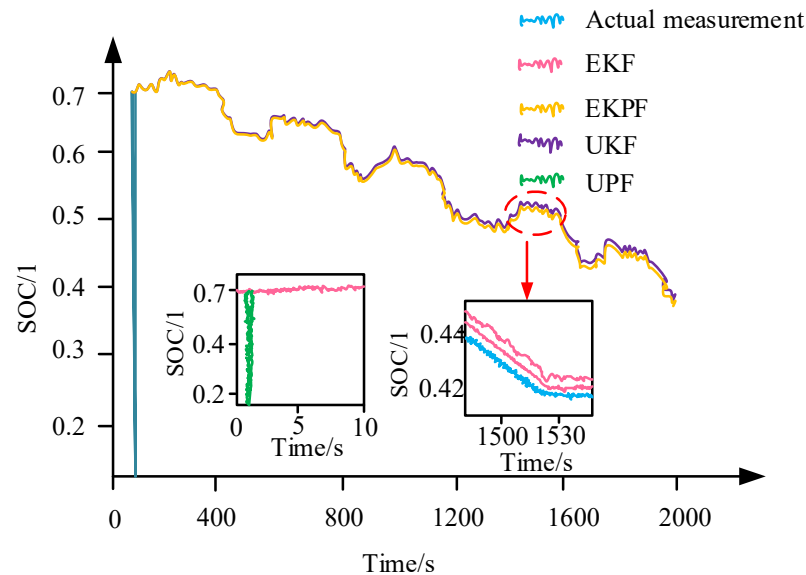


Figure 11. Algorithm estimation robustness at a SOC initial value of 0.2.

In Figure 11, the robustness of the algorithm estimation at an initial SOC value of 0.2 was not as good as that of the UKF at 1600 s.

4. Discussion

With the increasingly serious problem of global climate change, reducing the use of fossil fuels and promoting the development of renewable energy technologies have become an urgent task [25]. Electric vehicles, with their zero emissions, low noise and low maintenance costs, are considered to be a strong alternative to traditional fuel vehicles. However, despite significant advances in electric vehicle technology, the performance monitoring and management of their battery systems remains one of the key challenges. Lithium-ion batteries, especially ternary lithium batteries, are widely used in electric vehicles due to their high energy density and long cycle life. The state of Charge (SOC) of a battery is an important indicator to evaluate the remaining available energy of a battery, which is crucial to ensure the safety of electric vehicles, optimize energy management and extend battery life [26]. However, estimating SOC accurately is not easy. Complex electrochemical reactions inside the battery, changes in external operating conditions (such as temperature, aging), and nonlinear characteristics during charge and discharge all increase the difficulty of SOC estimation. Traditional SOC estimation methods, such as ampere-hour integration method and open-circuit voltage method, are simple and feasible, but their accuracy is limited in the face of complex working conditions and battery aging [27]. Therefore, the aim of this study is to develop a more accurate and reliable SOC estimation method to address the various challenges faced by electric vehicles in practical applications. By building a detailed model of ternary lithium batteries and using advanced filtering algorithms (such as UKF and UPF), it is expected to achieve accurate and real-time estimation of SOC, thereby providing strong support for battery management systems and promoting the further development of electric vehicle technology.

This study analyzed the SOC estimation of ternary lithium battery based on UKF, and the experimental results showed that UKF algorithm could accurately estimate the SOC of ternary lithium battery under intermittent discharge condition. Although its initial

reaction is not particularly fast, once it converges, it provides a relatively accurate estimate of SOC. This finding validates the effectiveness of UKF in nonlinear system state estimation, especially when dealing with complex systems such as ternary lithium batteries. This result is consistent with the conclusion obtained by Zhao et al. in their study on SOC valuation [28]. In addition, the experimental results show that the UPF algorithm has superior performance in the estimation of ternary lithium battery SOC. Compared with UKF algorithm, UPF algorithm can still maintain smaller estimation error under different parameter identification errors, and has stronger robustness and interference suppression ability. This coincides with the conclusion obtained by Liu's team in their research [29]. Finally, this study also found that the UPF algorithm has a significant improvement in the maximum absolute value of the estimation error, and the overall estimation effect is more stable. These advantages make UPF algorithms have greater potential in dealing with complex conditions and battery aging. The results are also similar to what Yetik found in his 2020 study of UPF algorithms [30].

This study focuses on the performance difference between UKF algorithm and UPF algorithm in SOC estimation of ternary lithium batteries. However, in practical applications, the battery management system also needs to consider other factors, such as the aging of the battery, temperature changes, and charge and discharge rates. These factors can affect the accuracy of SOC estimates. Therefore, future research can be further expanded to SOC valuation methods considering the comprehensive influence of multiple factors.

5. Conclusions

Although ternary LIPs are increasingly widely used in EVs, accurately estimating the pack's SOC in real-time remains a challenge. To address this issue, a ternary LPA model was constructed, and methods on the grounds of the UKF and the UPF for SOC estimation were subsequently adopted. By analyzing the performance comparison results of RMSE, the UPF increased by 50.9% compared to EKF, 33.4% compared to EKPF, and 19.6% compared to the UKF. The algorithm estimation robustness at an initial SOC value of 0.2 was not as good as that of the UKF at 1600 s. The maximum absolute error was also controlled from around 3% of EKF to within 1%, but it was relatively slow in running time. However, it should be noted that the UPF method has a high computational complexity and will require optimization and appropriate hardware support in practical applications. Overall, the potential of the UPF as an effective and robust SOC valuation method has been confirmed, and it may have broad application prospects for the ternary LPA and other types of packs. This may provide an important theoretical basis for improving the energy management efficiency, pack life, and overall vehicle performance of EVs in the future.

Author Contributions: Investigation, H.L.; Writing—original draft, Y.H.; Project administration, H.H. All authors have read and agreed to the published version of the manuscript.

Funding: The research is supported by the Science and Technology Research Project of the Chongqing Municipal Education Commission, 2022.7.1–2025.7.1. The project is also supported by the Scientific and Technological Research Program of Chongqing Municipal Education Commission: Research on State of Charge Estimation and Health Status Diagnosis of Vehicle Power Batteries (Grant No. KJQN202203411).

Institutional Review Board Statement: Not applicable.

Informed Consent Statement: Not applicable.

Data Availability Statement: The data presented in this study are available on request from the corresponding author. The data are not publicly available due to privacy.

Conflicts of Interest: Hu Huang is an employee of Seres Group Co., Ltd. The paper reflects the views of the scientists, and not the company. The authors declare no conflict of interest.

References

1. Ibrahim, K.S.M.H.; Huang, Y.F.; Ahmed, A.N.; Koo, C.H.; El-Shafie, A. Forecasting multi-step-ahead reservoir monthly and daily inflow using machine learning models based on different scenarios. *Appl. Intell.* **2022**, *53*, 10893–10916. [\[CrossRef\]](#)
2. Caian, G.; Yanping, Z.; Yang, Y. Comparison of two combined algorithms for SOC estimation of ternary lithium battery. *J. Chongqing Univ. Technol.* **2022**, *36*, 29–35.
3. Ming, T.T.; Zhao, J.; Wang, X.L.; Wang, K. SOC estimation of a lithium battery under high pulse rate condition based on improved LSTM. *Power Syst. Prot. Control* **2021**, *49*, 144–150.
4. Wang, Z.; Wang, S.; Yu, C.; Qiao, J. Improved Long Short-Term Memory: Statistical Regression Model for High Precision SOC Estimation of Lithium-Ion Batteries Adaptive to Complex Current Variation Conditions. *J. Electrochem. Soc.* **2023**, *170*, 050521. [\[CrossRef\]](#)
5. Hao, X.; Wang, S.; Fan, Y.; Xie, Y.; Fernandez, C. An improved forgetting factor recursive least square and unscented particle filtering algorithm for accurate lithium-ion battery state of charge estimation. *J. Energy Storage* **2023**, *59*, 106478. [\[CrossRef\]](#)
6. Lipu, M.H.; Hannan, M.; Karim, T.F.; Hussain, A.; Saad, M.H.M.; Ayob, A.; Miah, S.; Mahlia, T.I. Intelligent algorithms and control strategies for battery management system in electric vehicles: Progress, challenges and future outlook. *J. Clean. Prod.* **2021**, *292*, 126044. [\[CrossRef\]](#)
7. Xin, S.; Shan, H.; Vilsen, S.B. A review of non-probabilistic machine learning-based state of health estimation techniques for lithium-ion battery. *Appl. Energy* **2021**, *300*, 117346.
8. Li, P.; Xia, X.; Guo, J. A review of the life cycle carbon footprint of electric vehicle batteries. *Sep. Purif. Technol.* **2022**, *296*, 121389. [\[CrossRef\]](#)
9. Bhattacharyya, H.S.; Choudhury, A.B.; Chanda, C.K. On-road estimation of state of charge of lithium-ion battery by extended and dual extended Kalman filter considering sensor bias. *Int. J. Energy Res.* **2022**, *46*, 15182–15197. [\[CrossRef\]](#)
10. Juqiang, C.F.; Long, W.; Kaifeng, H. Online SOC estimation of a lithium-ion battery based on FFRLS and AEKF. *Energy Storage Sci. Technol.* **2021**, *10*, 242–249.
11. Sheikh, S.S.; Anjum, M.; Khan, M.A.; Hassan, S.A.; Khalid, H.A.; Gastli, A.; Ben-Brahim, L. A Battery Health Monitoring Method Using Machine Learning: A Data-Driven Approach. *Energies* **2020**, *13*, 3658. [\[CrossRef\]](#)
12. John, S.J.; Suma, P.; Athira, T.M. Multiset modules. *J. Comput. Cogn. Eng.* **2022**, *1*, 37–41. [\[CrossRef\]](#)
13. Alcantud, J.C.R. Convex soft geometries. *J. Comput. Cogn. Eng.* **2022**, *1*, 2–12. [\[CrossRef\]](#)
14. Camargos, P.H.; dos Santos, P.H.; dos Santos, I.R.; Ribeiro, G.S.; Caetano, R.E. Perspectives on Li-ion battery categories for electric vehicle applications: A review of state of the art. *Int. J. Energy Res.* **2022**, *46*, 19258–19268. [\[CrossRef\]](#)
15. Schaltz, E.; Stroe, D.-I.; Norregaard, K.; Ingvaridsen, L.S.; Christensen, A. Incremental Capacity Analysis Applied on Electric Vehicles for Battery State-of-Health Estimation. *IEEE Trans. Ind. Appl.* **2021**, *57*, 1810–1817. [\[CrossRef\]](#)
16. Baccouche, I.; Jemmali, S.; Manai, B.; Nikolian, A.; Omar, N.; Ben Amara, N.E. Li-ion battery modeling and characterization: An experimental overview on NMC battery. *Int. J. Energy Res.* **2022**, *46*, 3843–3859. [\[CrossRef\]](#)
17. Houache, M.S.; Yim, C.H.; Karkar, Z.; Abu-Lebdeh, Y. On the current and future outlook of battery chemistries for electric vehicles—Mini review. *Batteries* **2022**, *8*, 70. [\[CrossRef\]](#)
18. Dunn, J.; Slattey, M.; Kendall, A.; Ambrose, H.; Shen, S. Circularity of Lithium-Ion Battery Materials in Electric Vehicles. *Environ. Sci. Technol.* **2021**, *55*, 5189–5198. [\[CrossRef\]](#)
19. Shafique, M.; Akbar, A.; Rafiq, M.; Azam, A.; Luo, X. Global material flow analysis of end-of-life of lithium nickel manganese cobalt oxide batteries from battery electric vehicles. *Waste Manag. Res.* **2023**, *41*, 376–388. [\[CrossRef\]](#)
20. Tran, M.K.; DaCosta, A.; Mevawalla, A.; Panchal, S.; Fowler, M. Comparative study of equivalent circuit models performance in four common lithium-ion batteries: LFP, NMC, LMO, NCA. *Batteries* **2021**, *7*, 51. [\[CrossRef\]](#)
21. White, J.L.; Gittleson, F.S.; Homer, M.; El Gabaly, F. Nickel and Cobalt Oxidation State Evolution at Ni-Rich NMC Cathode Surfaces during Treatment. *J. Phys. Chem. C* **2020**, *124*, 16508–16514. [\[CrossRef\]](#)
22. Phillip, N.D.; Westover, A.S.; Daniel, C.; Veith, G.M. Structural Degradation of High Voltage Lithium Nickel Manganese Cobalt Oxide (NMC) Cathodes in Solid-State Batteries and Implications for Next Generation Energy Storage. *ACS Appl. Energy Mater.* **2020**, *3*, 1768–1774. [\[CrossRef\]](#)
23. Mu, L.; Zhang, J.; Xu, Y.; Wei, C.; Rahman, M.M.; Nordlund, D.; Liu, Y.; Lin, F. Resolving Charge Distribution for Compositionally Heterogeneous Battery Cathode Materials. *Nano Lett.* **2022**, *22*, 1278–1286. [\[CrossRef\]](#) [\[PubMed\]](#)
24. Sun, X.; Luo, X.; Zhang, Z.; Meng, F.; Yang, J. Life cycle assessment of lithium nickel cobalt manganese oxide (NCM) batteries for electric passenger vehicles. *J. Clean. Prod.* **2020**, *273*, 123006. [\[CrossRef\]](#)
25. Li, L.; Ju, X.; Zhou, X.; Peng, Y.; Zhou, Z.; Cao, B.; Yang, L. Experimental Study on Thermal Runaway Process of 18650 Lithium-Ion Battery under Different Discharge Currents. *Materials* **2021**, *14*, 4740. [\[CrossRef\]](#) [\[PubMed\]](#)
26. Zhang, Q.S. Research on the effect of thermal runaway gas components and explosion limits of lithium-ion batteries under different charge states. *J. Energy Storage* **2022**, *45*, 103759. [\[CrossRef\]](#)
27. Li, H.; Wang, Y.; He, X.; Li, Q.; Lian, C.; Wang, Z. Effects of Structure Parameters on the Thermal Performance of a Ternary Lithium-Ion Battery under Fast Charging Conditions. *Energy Fuels* **2020**, *34*, 8891–8904. [\[CrossRef\]](#)
28. Zhao, C.; Wang, T.; Huang, Z.; Wu, J.; Zhou, H.; Ma, M.; Xu, J.; Wang, Z.; Li, H.; Sun, J.; et al. Experimental study on thermal runaway of fully charged and overcharged lithium-ion batteries under adiabatic and side-heating test. *J. Energy Storage* **2021**, *38*, 102519. [\[CrossRef\]](#)

29. Liu, W.; Xu, M.; Zhu, M. Design of a niobium tungsten oxide/C micro-structured electrode for fast charging lithium-ion batteries. *Inorg. Chem. Front.* **2021**, *8*, 3998–4005. [[CrossRef](#)]
30. Yetik, O.; Karakoc, T.H. Three-dimensional thermal study on lithium-ion batteries in a hybrid aircraft: Numerical and experimental investigations. *SAE Int. J. Aerosp.* **2020**, *13*, 213–224. [[CrossRef](#)]

Disclaimer/Publisher's Note: The statements, opinions and data contained in all publications are solely those of the individual author(s) and contributor(s) and not of MDPI and/or the editor(s). MDPI and/or the editor(s) disclaim responsibility for any injury to people or property resulting from any ideas, methods, instructions or products referred to in the content.